JACS
JOURNAL OF THE AMERICAN CHEMICAL SOCIETY

Article

pubs.acs.org/JACS

Metal-Catalyzed Chemical Reaction of Single Molecules Directly Probed by Vibrational Spectroscopy

Han-Kyu Choi, Won-Hwa Park, Chan-Gyu Park, Hyun-Hang Shin, Kang Sup Lee, and Zee Hwan Kim*

Department of Chemistry, Seoul National University, Seoul 08826, Korea

Supporting Information

ABSTRACT: The study of heterogeneous catalytic reactions remains a major challenge because it involves a complex network of reaction steps with various intermediates. If the vibrational spectra of individual molecules could be monitored in real time, one could characterize the structures of the intermediates and the time scales of reaction steps without ensemble averaging. Surface-enhanced Raman scattering (SERS) spectroscopy does provide vibrational spectra with single-molecule sensitivity, but typical single-molecule SERS signals exhibit spatial heterogeneities and temporal fluctuations, making them difficult to be used in single-molecule kinetics studies. Here we show that SERS can monitor the single-molecule catalytic reactions in real time. The surface-immobilized reactants placed at the junctions of well-defined nanoparticle−thin film structures produce time-resolved SERS spectra with discrete, step-transitions of photoproducts. We interpret that such SERS-steps correspond to the reaction events of individual molecules occurring at the SERS hotspot. The analyses of the yield, dynamics, and the magnitude of such SERS steps, along with the associated spectral characteristics, fully support our claim. In addition, a model that is based on plasmonic field enhancement and surface photochemistry reproduces the key features of experimental observation. Overall, the result demonstrates that it is possible, under well-controlled conditions, to differentiate the chemical and physical processes contributing to the single-molecule SERS signals, and thus shows the use of single-molecule SERS as a tool for studying the metal-catalyzed organic reactions.

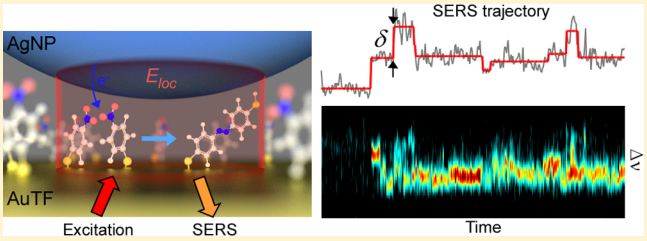

1. INTRODUCTION

The metal-catalyzed reaction is the most important but least understood topic in chemistry because of its particularly complex reaction mechanism. The single-molecule spectroscopy may enable us to identify the hidden reaction steps and intermediates constituting the reactions. Recently, single-molecule fluorescence (SMF) spectroscopy with specifically designed probes has been utilized to study the catalytic activities of nanoparticles.[1−6] The fluorescence spectra, however, carry insufficient structural information to fully identify various intermediates and products, severely limiting the scope of investigation. This missing molecular "fingerprint" may be obtained if the vibrational spectra of individual reacting molecules could be measured in situ.

The surface-enhanced Raman scattering spectroscopy (SERS)[7,8] provides vibrational spectra of unlabeled organic molecules on metallic surfaces. As such, from the very early days of SERS research, its use in in situ catalytic kinetics studies has been explored (for a comprehensive review, see ref 9 and references therein). Although the single-molecule sensitivity of SERS (single-molecule SERS, SMSERS)[10−21] has been discovered[11,12,22] and solidly *proved* recently,[13,14] it is still rarely applied to single-molecule reaction kinetics studies.[20,22−24] This is mainly caused by its stochastic temporal fluctuations,[11,15,17,22,25−27] which cannot be easily assigned to a specific type of molecular process. Furthermore, the SMSERS activities vary widely over the sample surfaces. Several sources, including the Brownian dynamics (translational and orientational diffusion) of a molecule placed near a hotspot,[25,28] the fluctuation of the state of the metallic surfaces,[25,26] and uncontrolled SERS hotspot geometries, are believed to give rise to the complexity. Despite such problems, a few recent kinetic studies show temporal signatures of SERS hinting the feasibility for single or a few molecule kinetics studies with SERS.[20,29]

The following questions thus arise: If we could remove or control all of these variabilities, would SMSERS provide predictable and quantifiable signals of individual molecules in a way that is as useful as, or even better than, SMF? Would the dynamic SMSERS measurement under this condition enable in situ monitoring of the single-molecule reactions occurring on metallic surfaces? Here we demonstrate that single molecules immobilized at the centers of plasmonic hotspots do generate fully predictable SMSERS signals, and that the time-resolved SERS signals of reacting molecules under such conditions yield remarkably clear temporal signatures of single-molecule reaction events. The signals thus obtained could be fully explained by the reaction of single molecules and their plasmon-enhanced Raman scattering. Current study is specifically focused on the dimerization of 4-nitrobenzenethiols,[30−36] which have been extensively studied at an ensemble level.

Received: February 19, 2016
Published: March 10, 2016

DOI: 10.1021/jacs.6b01865
J. Am. Chem. Soc. 2016, 138, 4673−4684

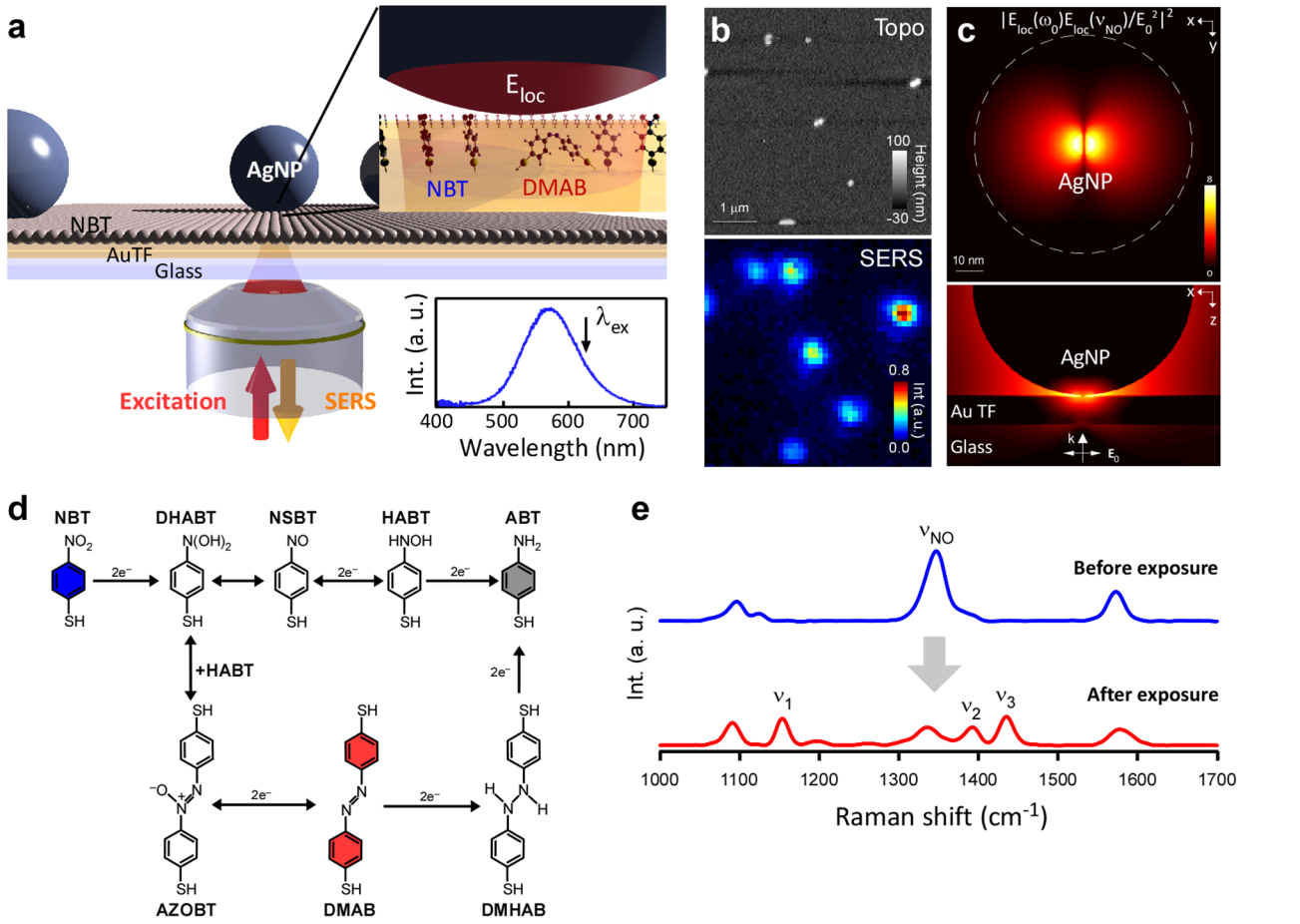

Figure 1. (a) Schematic diagram of a AgNP-NBT-AuTF junction, and SERS measurement. The inset shows the local field (E_{loc}), NBT, and DMAB, and a dark-field scattering spectrum obtained from a single AgNP-NBT-AuTF junction, and the laser wavelength (λ_{ex} = 632.8 nm, black arrow) for the SERS measurement. (b) Atomic force microscopy (AFM) topography (top-panel, Topo) and SERS (bottom panel, intensity of ν_{NO} = 1347 cm^{-1} peak of NBT) images of the sample, showing the locations of hotspots. (c) Top (*xy*-plane, top panel) and side (*xz*-plane, bottom panel) views of the theoretical electromagnetic enhancement factor, $|E_{loc}(\omega_0)E_{loc}(\omega_{NBT})/E_0^2|^2$. The color scale of the image is logarithmic. (d) Reaction pathways and possible intermediates for the photoinduced dimerization of NBT. The intermediates involved are dihydroxylaminobenzenethiol (DHABT), nitrosobenzenethiol (NSBT), hydroxylaminobenzenethiol (HABT), azoxybenzenethiol (AZOBT) and dimercaptohydroazobenzene (DMHAB). (e) SERS spectra of the sample before (blue) and after laser irradiation (red). For the former, the peak at 1347 cm^{-1} is ν_{NO} (symmetric NO stretching) of NBT. For the latter, the peaks at 1146 cm^{-1}, 1394 cm^{-1}, and 1445 cm^{-1} are assigned to the ν_1 (CH-bending), ν_2 (bending and stretching), and ν_3 (bending and stretching) modes of DMAB, respectively.

We nevertheless believe that the method we present should be also applicable to other metal-catalyzed reactions involving Raman-active chemical species.

2. RESULTS AND DISCUSSIONS

2.1. Localized Photocatalytic Reactions at a Plasmonic Junction. The sample (Figure 1a) is a self-assembled silver nanoparticle (AgNP, diameter of 80 nm)-4-nitrobenzenethiol (NBT)-gold thin film (AuTF, thickness of 10 nm)[27,37,38] junctions formed on a glass coverslip. As shown by many recent reports,[27,29,39−43] the NP-molecule-TF junctions show fairly reproducible Raman enhancements, offering a facile platform for SERS/SMSERS kinetic studies.[29] For the current work, the NBT serves both as a reagent and a spacer defining a plasmonic gap of 0.7 nm. A focused laser beam at λ_{ex} = 632.8 nm, resonating with the dipolar plasmon mode of the junction (see inset of Figure 1a for the scattering spectrum), locally drives the photoreduction of NBT to yield 4,4′-dimercaptoazobenzene (DMAB), a long-lived reaction intermediate, which is further reduced to 4-aminobenzenethiol (ABT).[20,30−35,44−50] The same laser also excites the SERS radiation of the reacting molecules, and the resulting SERS spectra are recorded in real-time. As shown in atomic force microscopy (AFM) and confocal SERS images (Figure 1b, ν_{NO}-peak intensity map of NBT. See also Figure 1e) of the sample, the SERS signal of NBT is strongly enhanced only at the AgNP-NBT-AuTF junction sites. The measured Raman enhancement factor of 1.7 × 10^8 could be reproduced within 1 order of magnitude by the local field (E_{loc}) enhancement around the junction (see Figure 1c and Supporting Information A).

It is believed that two reaction pathways are possible[20,30−35,44−49] for the reduction of NBTs (see Figure 1d). Through the direct path, NBT is reduced to aminobenzenethiol (ABT) via the series of reduction steps involving the dihydroxylaminobenzenethiol (DHABT), nitrosobenzenethiol (NSBT), and hydroxylaminobenzenethiol (HABT) intermediates. Through the indirect path, the DHABT and HABT condense to yield dimercaptoazobenzene (DMAB). The DMAB is further reduced to the ABTs. For the photocatalytic reaction, the electrons needed for each of the reduction steps are believed to come from hot-electrons[32,51−53] transferred from the nanostructures. The above mechanism is based on numerous

DOI: 10.1021/jacs.6b01865
J. Am. Chem. Soc. 2016, 138, 4673−4684

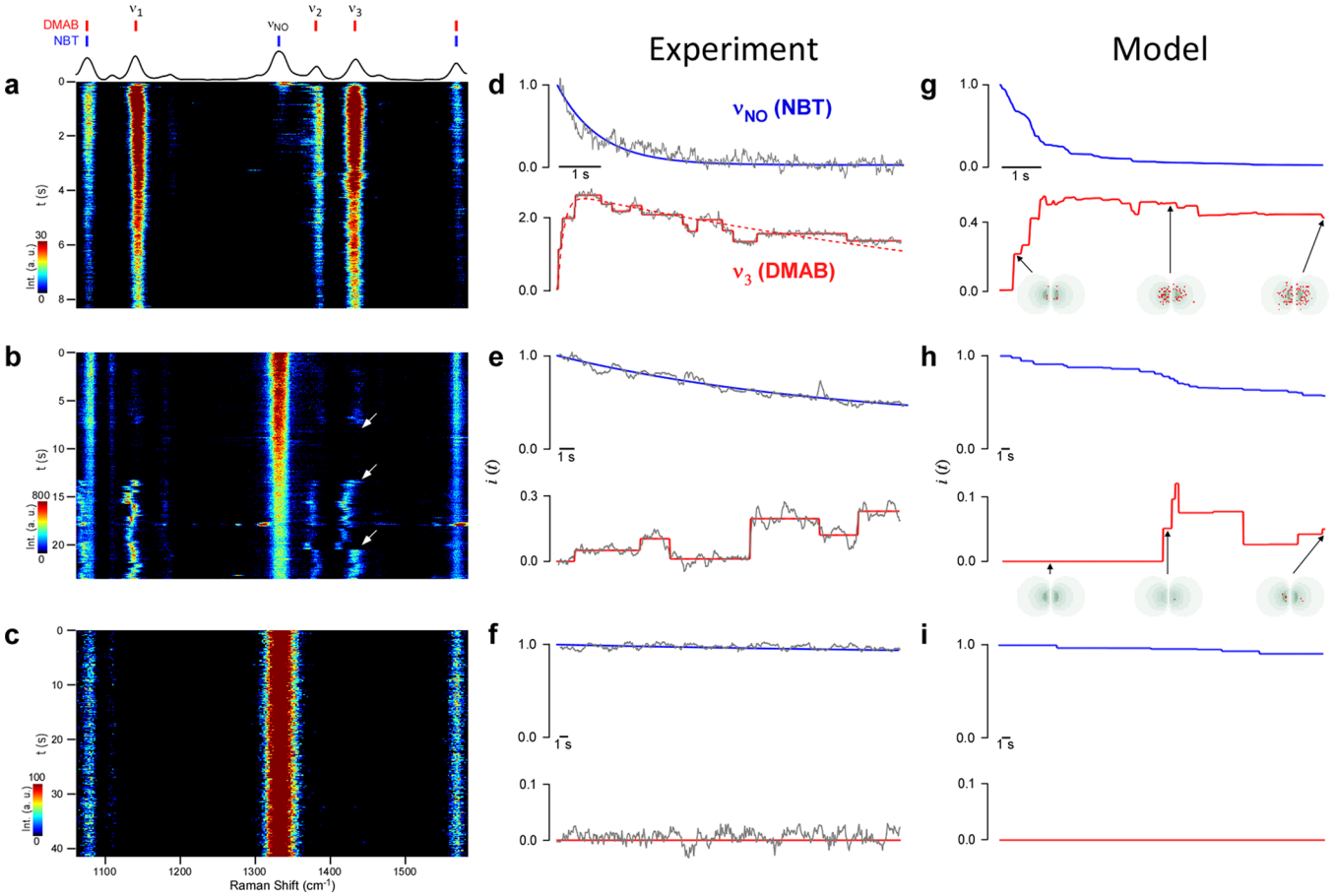

Figure 2. Time-resolved SERS trajectories. (a–c) Time-resolved SERS spectra of AgNP-NBT-AuTF junctions. The horizontal and vertical axes correspond to the Raman shift (in cm^{-1}) and time (in seconds), respectively, and the intensities of SERS peaks are presented as colored images (see inset color scales). White arrows in (b) point to the discrete changes in the SERS intensities of ν_3 (DMAB). The topmost inset shows the sample SERS spectrum obtained during the reaction, together with the peak assignment of NBT (blue) and DMAB (red). (d–f) Time-resolved SERS intensities (gray) of ν_{NO} (NBT) and ν_3 (DMAB) peaks sampled from (a–c), along with the fit to a single exponential function (blue) and step function (red). The dotted red trace in (d) is the fit to a rise-and-decay rate equation, showing that the envelope of the DMAB trajectory approximately follows the ensemble kinetics. In (d–i), the intensities shown are normalized with respect to the initial SERS intensity of the ν_{NO} (NBT) peak. (g–i) Model SERS trajectories of ν_{NO} (NBT, blue) and ν_3 (DMAB, red). The inset cartoons in (g) and (h) display snapshots of the DMAB distributions (red dots) and the local field distribution (green) on the junction.

electrochemical and SERS spectroscopic evidences, yet the relative importance of the two paths, or even the existence of DMAB as a reaction intermediate is still under debate.[54] While the major point of the current study is not on proving or disproving the proposed mechanism, we have obtained spectroscopic evidence (see below and Supporting Information B) strongly supporting that less than minor portion (<10%) of the NBTs undergo a dimerization reaction (indirect path) producing DMAB intermediate. Thus, in what follows, our interpretation of the data is based on the above-mentioned reaction mechanism.

Figure 1e shows SERS spectra recorded from a single junction, before (blue) and after (red) laser irradiation. The disappearance of the NO-stretching peak of NBT (ν_{NO} = 1347 cm^{-1}) and the appearance of three new peaks associated with *trans*-DMAB (below, we simply call it DMAB) at ν_1 = 1146 cm^{-1} (CH-bending), ν_2 = 1394 cm^{-1} (bending and stretching), and ν_3 = 1445 cm^{-1} (bending and stretching) indicates that NBTs undergo a reaction to yield DMAB (see Supporting Information C for peak assignment).

2.2. Reactive SERS Trajectories. *2.2.1. General Features.* Figure 2a–c show three representative time-resolved SERS spectra obtained from individual junctions similar to those described in Figure 1. The Figure 2d–f present the corresponding SERS intensity trajectories of the ν_{NO} (NBT) and ν_3 (DMAB) peaks. The data set shows two major features. First, the trajectories from different junctions show widely different dynamics for NBT and DMAB, and the two are temporally correlated: The ones showing fast NBT decay (blue traces in Figure 2d–f represent the fit to a single-exponential decay, $\exp(-k_{NBT}t)$, where t is the time and k_{NBT} is the decay constant) are associated with a strong DMAB intensity (Figure 2a and d, called hot trajectories), whereas the ones showing slow NBT decay are associated with weak (Figure 2b and e, mild trajectories) or zero (Figure 2c and f, cold trajectories) DMAB intensities. Second, a majority of DMAB-forming trajectories (Figure 2a, b, d, e) show step-like transitions in the ν_1, ν_2, and ν_3 peaks of DMAB (red traces in Figure 2d–f represent fits to step-functions:[55] See below for more detail). Such transitions are most notable in the mild trajectories (Figure 2b and e, see white arrows), in which the intensities and spectra show a few clear on/off transitions of the DMAB peaks. In the hot trajectories of DMAB (Figure 2a and d), many such steps are rapidly accumulated to produce an overall envelope that

DOI: 10.1021/jacs.6b01865
J. Am. Chem. Soc. 2016, 138, 4673–4684

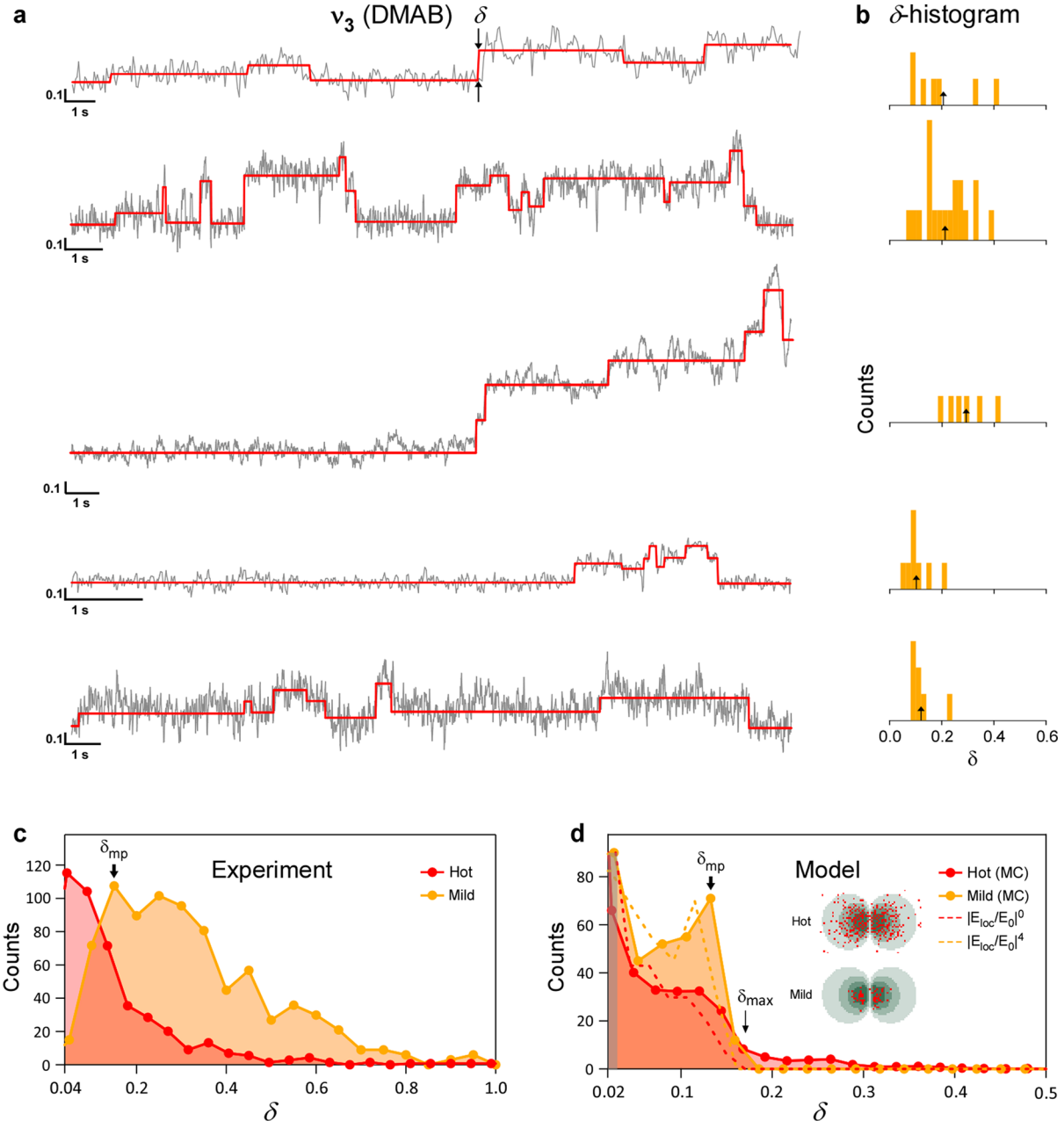

Figure 3. Discrete steps in the SERS trajectory of DMAB. (a) Normalized SERS trajectories of ν_3 (DMAB), i_{DMAB} (gray trace), of mild junctions, and the fits to step-functions (red). The horizontal and vertical scale bars represent 1 s and 0.1 (normalized intensity unit), respectively. (b) Histograms of the step size (δ, indicated in arrows in the top panel of (a)) extracted from each of the trajectories shown in (a). The black arrows point to the average step size for each trajectory. (c) δ-distributions accumulated from the mild (orange) and hot (red) trajectories. (d) δ-distributions for the mild (k_{NBT} = 0.025 s^{-1}) and hot (k_{NBT} = 1.4 s^{-1}) trajectories derived from Monte Carlo simulation (see Figure 8d). Also shown in dashed lines are the δ-distributions evaluated from a nonuniform DMAB distribution proportional to $|E_{loc}(x, y, \omega_0)/E_0|^4$ and from a uniform DMAB distribution ($|E_{loc}(x, y, \omega_0)/E_0|^0$). The δ_{max} = 0.17 indicates the theoretical maximum step size. The shaded region in (d) corresponds to the range of δ that is experimentally inaccessible. The inset in (d) displays cumulative spatial distributions of DMABs (red dots) produced during the reaction, and the local field distribution (green) calculated for hot and mild trajectories.

approximately follows an ensemble rise-and-decay rate equation (red dashed curve). We attribute that the discrete changes in SERS intensities correspond to the creation and annihilation of individual DMABs within a hotspot, and their time-evolution represents the single-molecule reaction kinetics. As mentioned above, a majority of NBTs take the direct reaction path rather than the indirect, DMAB-forming, path. This explains why the NBT trajectories show continuous decay, whereas the DMAB trajectories show discrete changes. The minority event (<10%) of DMAB formation is readily recognized in the SERS spectra, because the Raman cross section of DMAB is significantly larger than those of ABT and NBT (σ_{DMAB} (1445 cm^{-1}):σ_{NBT} (1347 cm^{-1}):σ_{ABT} (1069 cm^{-1}) = 46.6:12.6:1.0, see Supporting Information D).

2.2.2. Rate-Law Analysis of Hot SERS Trajectories. The hot SERS trajectories most likely represent the kinetics of an ensemble of NBT and DMAB, because the DMAB intensity profiles as well as those of the NBT could be satisfactorily fitted

DOI: 10.1021/jacs.6b01865
J. Am. Chem. Soc. 2016, 138, 4673−4684

to the standard rate law equations ($\exp(-k_{NBT}t)$ for NBT, and $\exp(-k_2t) - \exp(-k_3t)$ for DMAB). From the fitting (Supporting Information E), we find that the three rate constants (k_{NBT}, k_2, and k_3) are linearly proportional to the square-root of the initial intensity of ν_{NO} of NBT ($I_{0,NBT}$), and thus to the local-field intensity averaged over the junction area, $\langle|E_{loc}(\omega_0)|^2\rangle$ (where ω_0 is the excitation laser frequency). This supports that the associated reaction steps are one-photon processes and that major source of junction-to-junction variation of rates is the variation in E_{loc}. Additionally, we find that the k_3 (buildup rate of DMAB) is essentially the same as $2k_{NBT}$, indicating that the formation rate of DMAB is primarily limited by the (slow) decay of NBT to form reaction intermediates.

2.2.3. SERS Steps. For the quantitative analysis of SERS steps, we use the SERS intensity of the DMAB peak (ν_3, $I_{DMAB}(t)$) normalized by the initial intensity of the NBT peak (ν_{NO}, $I_{0,NBT}$): $i_{DMAB}(t) = I_{DMAB}(t)/I_{0,NBT}$ (below, we use the peak at ν_3 = 1445 cm^{-1} as the primary marker of DMAB, although the two other peaks also carry similar information as well). Here, the $I_{0,NBT}$ serves as an internal reference for SERS activities for each junction. Figure 3a displays a representative collection of $i_{DMAB}(t)$ with k_{NBT} < 0.1 s^{-1} (mild trajectories) along with fits to step-functions. From the fitting, we obtain the magnitude of the step (δ) in $i_{DMAB}(t)$ (see arrows in Figure 3a). For the step-fitting, the detector noise of the spectrometer sets a minimum detectable step-size of δ_{min} = 0.03, and any features smaller than this value are ignored in the analysis.

Figure 3b shows the δ-histograms extracted from the trajectories shown in Figure 3a. Notably, we find that the δ's in a given trajectory span a finite range, although the average δ's for each trajectory (shown as arrows) are similar. Figure 3c (orange) shows the δ-histogram accumulated from 17 mild trajectories (k_{NBT} = 0.005–0.1 s^{-1}), including the ones shown in Figure 3a, displaying a distribution spanning a range of δ = 0.03–0.8, with the most probable step size of δ_{mp} = 0.15. An analogous analysis of hot trajectories (k_{NBT} = 0.1–4.3 s^{-1}) yields a distribution (Figure 3c, red trace) spanning a comparable δ-range but with a monotonically decreasing shape. We attribute that the finite width in δ-distribution arises from the individual DMABs created at different lateral positions with respect to the junction center, experiencing different E_{loc}-intensities, thus creating a range of single-molecule SERS intensities. The difference in δ-distributions of hot and mild trajectories arises from different spatial distribution of DMABs arising from different reaction conditions. In this section, we present a series of experimental and theoretical proofs to the above claims.

2.3. Experimental Proofs for Single-Molecular Reaction Events. Here, we present the photochemical and spectroscopic features of experimental data answering to the following two questions: Do the SERS steps represent single-molecule signals of DMABs? If they do, do the time-evolutions of the steps represent the single-molecule reaction kinetics, or the Brownian dynamics (lateral diffusion or reorientation)?

2.3.1. Photochemical Proofs. We rely on two obvious characteristics of single-molecule kinetics and spectroscopy: First, if the steps are really the SERS intensity "quanta" of single-molecule reaction products, change in reaction condition may change the yield (overall occurrence probability) of the steps, yet the magnitudes of the individual steps should remain unchanged. Second, if the time-evolution of the steps represents the genuine single-molecule kinetics, the temporal dynamics of steps, on the average, should follow similar trends as is found in the corresponding ensemble kinetics.

Influence of Initial Reagent Coverage on the Yield of DMAB Steps. We systematically change the initial coverage of NBT, and examine the change in the yield and average magnitude of DMAB SERS steps, which is analogous to the "dilution" experiment by Weckhuysen and co-workers.[54] The plasmonic junctions with a mixed monolayer of NBT and benzenethiol (BT) with varying initial relative mole fractions ($\theta_{NBT}^0 + \theta_{BT}^0 = 1$) are prepared, and the SERS trajectories similar to the ones in Figure 3a are measured for multiple number of junctions. Here, the BT serves as a nonreactive, immobile diluent.

Figure 4 summarizes the result, highlighting three important features. First, we observe (Figure 4a, bar graph) that the yield

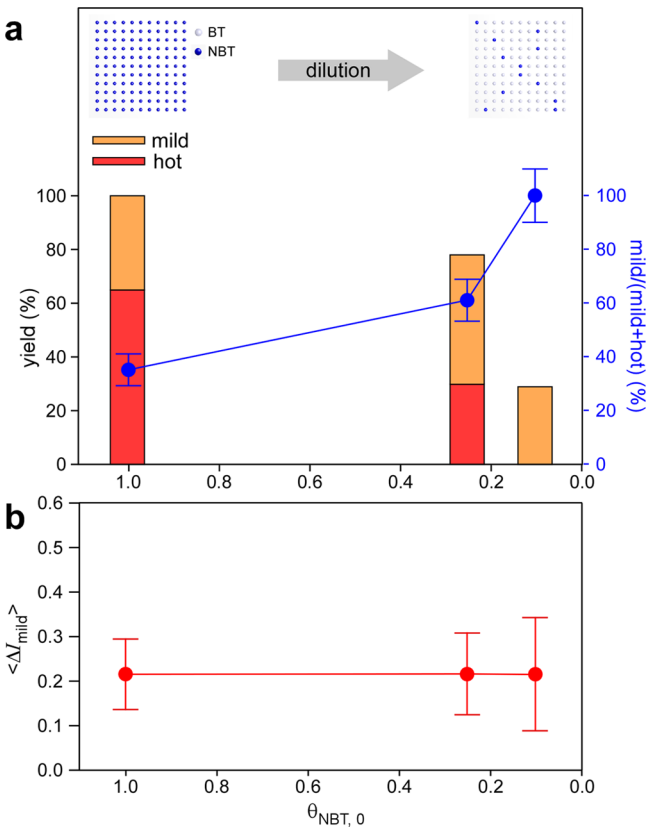

Figure 4. The change of yield and the magnitude of DMAB SERS steps as a function of initial NBT coverage. (a) (left y-axis and bar-graphs): Fraction of junctions yielding DMAB products (orange = mild, red = hot) plotted as a function of initial surface coverage of NBT (θ_{NBT}^0). (right y-axis and blue circles): Fraction of mild trajectories among the reactive trajectories. (b) The average size of unnormalized DMAB steps for different θ_{NBT}^0. The error bars represent one standard deviation of replicate measurements on different junctions.

of DMAB, which is defined as the fraction of DMAB-forming junctions ($(N_{mild} + N_{hot})/N_{tot}$, where N_{mild}, and N_{hot} are the numbers of junctions yielding mild and hot trajectories, respectively, and the N_{tot} is the total number of junctions examined), rapidly decreases upon dilution (decrease in θ_{NBT}^0). This proves that the SERS peaks of DMAB arise from the bimolecular association of photogenerated intermediates. At the same time, however, we observe that the dilution does not significantly change the decay rate (k_{NBT}) of the NBT peaks

DOI: 10.1021/jacs.6b01865
J. Am. Chem. Soc. 2016, 138, 4673–4684

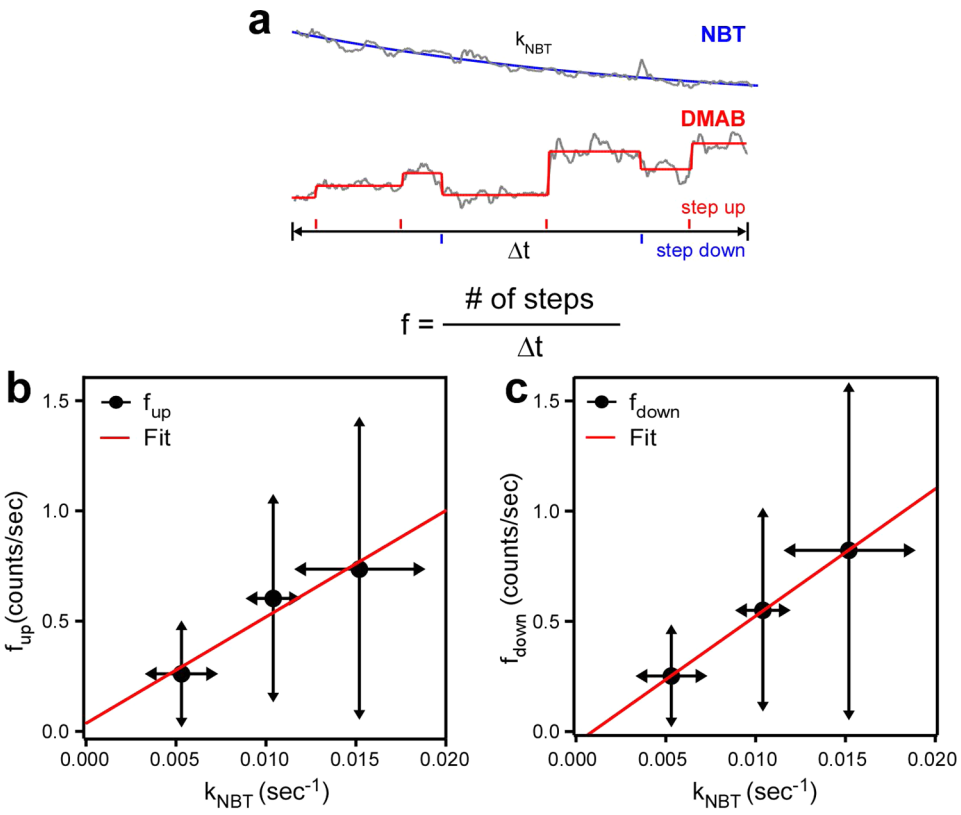

Figure 5. Dynamics of DMAB step-transitions and its correlation to the reagent decay dynamics. (a) A representative SERS trajectory showing the NBT decay (k_{NBT}) and the steps, along with fits to exponential and step functions. The up-step and down-step transitions are indicated as red and blue vertical bars, respectively. The stepping frequency, f, is defined as the number of steps within a unit time. (b) Correlations (black circles) of step-up frequency (f_{up}) and k_{NBT}. (c) Correlation of step-down frequency (f_{down}) and k_{NBT}. A total of 24 trajectories are analyzed, and the raw (k_{NBT}, $f_{up,down}$)-points (see Supporting Information F) are binned into three sets based on the range of k_{NBT}: $0.003 < k_{NBT} < 0.009$ (7 trajectories); $0.010 < k_{NBT} < 0.012$ (6 trajectories); $0.013 < k_{NBT} < 0.090$ (11 trajectories). The data points shown in (b,c), and the associated error bars (vertical and horizontal double-sided arrows) correspond to the average and the standard deviation of each binned data sets. As such, the y-error bars represent both the variation of $f_{up,down}$ for a given k_{NBT}, and the range of data binning. The red lines in (b) & (c) are the linear fit to the data.

(Figure S5 of Supporting Information E), confirming that the NBT decay step corresponds to the generation of monomeric intermediates, not to the direct one-step dimerization of the two NBTs.

Second, while the dilution decreases overall yield of the DMAB, it does increase the fraction of mild trajectories among the total number of reactive trajectories, $N_{mild}/(N_{mild} + N_{hot})$ (Figure 4a, blue dot and line): for the sample with $\theta_{NBT}{}^{0} = 1.0$, 35% of the reactive trajectories appear as mild trajectories, whereas for the ones with $\theta_{NBT}{}^{0} = 0.1$, all of the reactive trajectories appear as mild trajectories. This agrees with our hypothesis that the mild trajectories simply represent the fewer-molecule limit of the same chemical reaction as is occurring in hot trajectories: Dilution makes it less probable to find two neighboring intermediates for the dimerization, and thus a majority of the DMAB signals appear as discrete single molecular events.

Third, and the most importantly, we find that the average step sizes for mild trajectories remain unchanged upon dilution (see Figure 4b. For the plot shown in Figure 4b, the step intensities are not normalized with respect to $I_{0,NBT}$ in order to avoid any possible analysis bias). This further supports that the steps are the SERS signals of individual molecules, the magnitude of which is unaffected by the reaction condition. If the steps were originated from collective changes of an ensemble of DMAB molecules, the step sizes should *decrease* in proportion to the degree of dilution. To better understand the logic behind this argument, we consider a hypothetical situation where an ensemble of molecules contributes to the stepped SERS trajectory. Discrete spectroscopic signatures may be obtained *only if* the changes of local environment (for example, change in metallic surface states) lead to the collective modulation of the number density of molecules, Raman enhancement, or the orientation of *all* of the molecules under such environment. Alternatively, the discrete signals may arise from the time-averaged signals of bursts of single-molecular reaction events (multicount) occurring at a time scale much faster than the acquisition time of spectra (~30 ms). If the collective or multicount events are the dominant source of the steps, the dilution of the reagent will decrease the number of molecules contributing to the transitions, and thus systematically decrease the magnitude of steps. Our observation indicates otherwise, and thus supports that the steps are the SERS signals of individual molecules. Overall, the yield and the magnitude of the SERS steps strongly support that the DMAB steps aries from the individual molecules produced by bimolecular surface chemical reaction.

Dynamics of SERS Steps and Possible Roles of Brownian Motion. As described above, the rate constants of NBT decay (k_{NBT}), and rise and decay of DMAB (k_2 and k_3) for each hot trajectories are linearly proportional to each other. If the stepped transitions in mild trajectories represent the dynamics

DOI: 10.1021/jacs.6b01865
J. Am. Chem. Soc. 2016, 138, 4673−4684

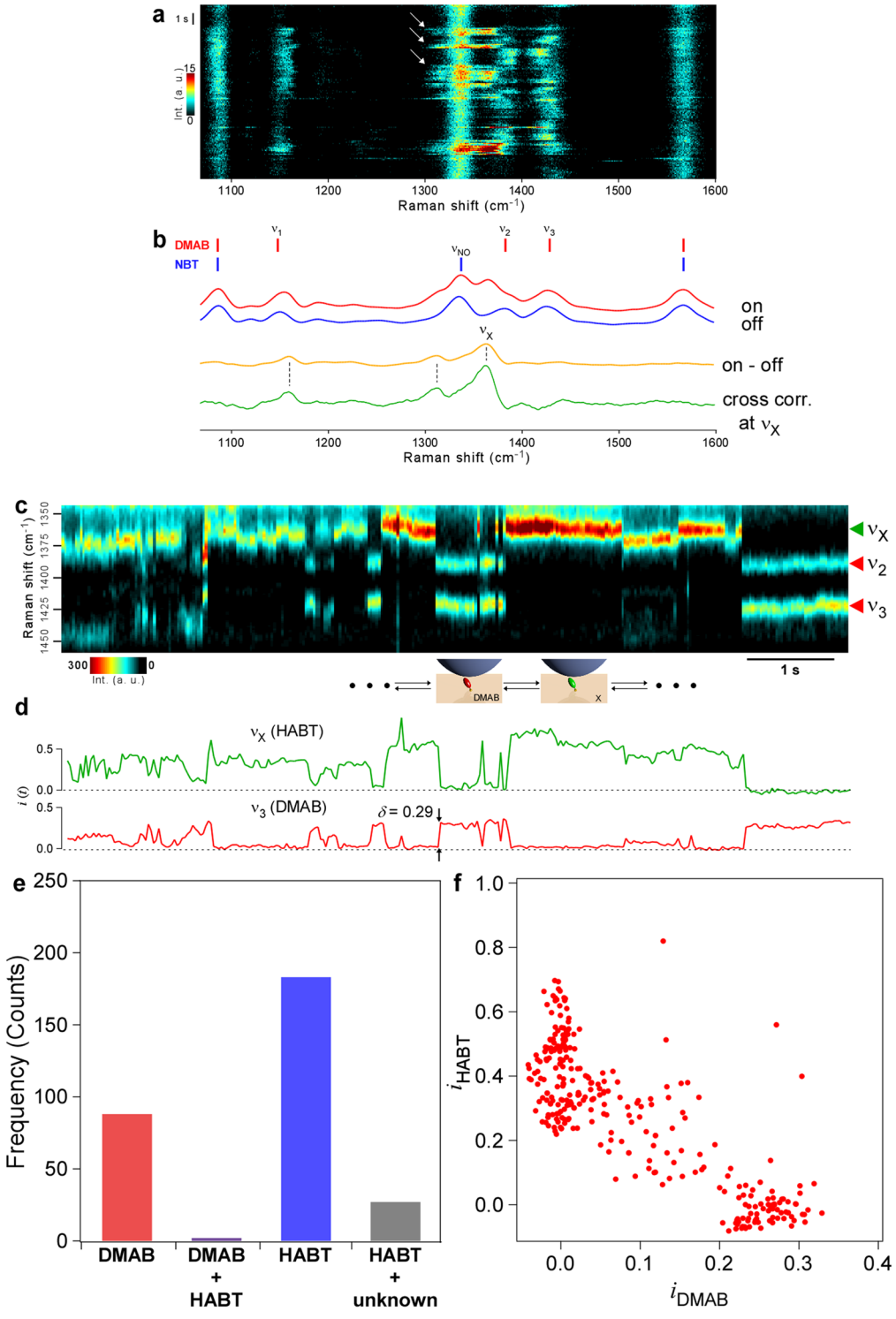

Figure 6. Bianalyte analysis of reactive SERS trajectory. (a) A mild trajectory showing the intermittent (on/off) spectral signature of an intermediate (see white arrows). (b) SERS spectra sampled from (a) during the on (red), and off (blue) periods. Also shown are the difference of the two (on−off, orange), and the ν_X = 1364 cm^{-1} component of the 2D covariance matrix (green, see Supporting Information H for more detail), both of which showing peaks at 1364, 1160, and 1314 cm^{-1}, which are assigned as the vibrational peaks of HABT (vertical dotted lines). (c) A SERS trajectory showing the peak at ν_X = 1364 cm^{-1}, which is anticorrelated to the peaks of ν_2 and ν_3. (d) Corresponding intensity trajectories of ν_3 (DMAB) and the ν_X (HABT). (e) Event histogram derived from (c), showing the statistics of pure-DMAB (red), pure HABT (blue), DMAB + HABT (purple), and HABT + unknown (gray) events. (f) intensity−intensity correlation of the peaks at ν_3 = 1445 cm^{-1}, and ν_X = 1364 cm^{-1}, showing two clearly identifiable distributions for single molecular events of DMAB and HABT.

of formation (up-step) and the annihilation (down-step) of individual DMAB, the frequency of step-transitions (f = number of steps/unit time) and k_{NBT} for a given trajectory should also correlate to each other linearly. If, on the other hand, a majority of step-transitions arise from the single-molecule Brownian dynamics (lateral diffusion and reorientation),[56] which is

DOI: 10.1021/jacs.6b01865
J. Am. Chem. Soc. 2016, 138, 4673−4684

unrelated to the chemical reaction, the rate of step-transitions will be nearly independent of k_{NBT}. In Figure 5, we show the correlation plots of (k_{NBT}, f_{up}) and (k_{NBT}, f_{down}) both of which show clear linear relationships with the linear fits extrapolating to near-zero y-intercept. Therefore, we believe that the step-transitions mainly arise from the reaction events, not from the single-molecule Brownian dynamics. Note that organic thiolates covalently bonded to Au have a very short diffusion length (rms displacement of 0.02 nm in 1 s[57]). As such, the lateral diffusion of the molecules in and out of SERS hotspot (spanning an area with ∼10 nm diameter) in the time scale of a few tens of seconds is highly unlikely. Temporarily blocking and unblocking the laser beam during the reaction (for >10 min, see Supporting Information G) leaves the SERS intensities of NBT (and DMAB) essentially unchanged, further supporting that the diffusion of thiolates in and out of the hotspot is negligible. The reorientation dynamics may still manifest itself in the statistical scatter (error bars) in correlation plots in Figure 5b and c, and also in the fast fluctuation of SERS signals (<10 ms) superimposed on top of the stepped transitions.

2.3.2. Spectroscopic Proofs. Bianalyte Analysis. Here we employ the bianalyte SERS approach,[13,14] which is the most widely accepted statistical tool for assessing the single-molecular events in SERS, to further prove that the stepped transitions arise from individual molecules. In the standard bianalyte method, the SERS peak intensities of the mixture of two species (called the A and B) are measured as a function of time or position. If the statistics of the pure events (A-only or B-only spectra) dominate over the mixed events (spectra showing the features of both A and B), one can statistically argue that the hotspot contains 0 or 1 molecules at any given time. In an ideal situation where we have exactly one A- or one B-molecule in hotspot area, and where the detection time scale is much faster than the reaction time scale, the probability to find the mixed A+B event is identically zero.

In this work, we have compared the SERS spectra of DMAB (A) and the short-lived reaction intermediate (B) recorded during the reaction. Some of the mild trajectories with very small k_{NBT} (<0.001 s^{-1}) show (Figure 6a and b) intermittent SERS peaks at 1160, 1314, and 1364 cm^{-1}, which cannot be assigned to any of the vibrational modes of NBT, DMAB or ABT. These peaks are consistently observed in ∼20% of the mildest trajectories, and thus are most likely to originate from the reaction. Furthermore, the intensities of such peaks and those of DMABs are temporally anticorrelated. Cross correlation analysis[58] (Supporting Information H) further confirms that these three peaks originate from single chemical species (with covariance coefficients exceeding +0.7). On the basis of the density functional theory calculation (see Supporting Information I), we tentatively assign the structure of intermediate as HABT (for the purpose of the current study, exact identity of the intermediate is unimportant, however). Figure 6c displays a part of the time-resolved SERS spectra showing a peak at ν_X = 1364 cm^{-1}, together with the ν_2 and ν_3 peaks of DMAB. For the particular trajectory shown, the intensities of the ν_2 and ν_3 (DMAB) undergo on/off transitions (Figure 6d) with $\delta \sim 0.3$, and the new peak shows on/off transitions that are perfectly anticorrelated to the ν_2 and ν_3 intensities, such that there is very small probability for simultaneous appearance of the DMAB and the HABT at any given time. Similar two-state spectral signatures in single-molecule tip-enhanced Raman scattering have been recently observed for the azobenzene derivatives[59] and malachite green.[60]

The associated event histogram shown in Figure 6e is categorized as pure-DMAB (showing peaks at both ν_2 and ν_3 positions), pure-HABT (showing a peak at ν_X), DMAB + HABT (showing the ν_2, ν_3, and ν_X), and HABT + unknown (showing ν_X and other unidentifiable spectral features), showing negligibly small probability of mixed event as compared with DMAB-only or HABT-only events. The bianalyte analysis shown above clearly proves that the step structure with δ = 0.29 is a strictly single-molecular event (note that even the two-molecular event has larger statistical weight than the pure events). Another notable feature of the trajectory is that the trajectories maintain fairly constant on-state intensities of DMAB and HABT even after several on/off cycles (see Figure 6d), which strongly suggesting that the positions of DMAB and HABT remain nearly unchanged during these transitions. Such characteristics are better illustrated in intensity−intensity correlation diagram of ν_3 and ν_X peaks (Figure 6f), in which two clearly defined distributions near (i_{DMAB}, i_X) = (0.27, 0.0) and (0.0, and 0.4) account for >90% of the events. This is fully consistent with a reversible chemical transformation between a single DMAB and a single HABT, occurring at the same surface site. Most of the remaining mixed events (accounting for ∼0.7%) are positioned near the line connecting the centers of the two distributions. The most straightforward explanation is that these are the points where the DMAB-HABT transitions have occurred during the time-window of data acquisition, resulting in spectral mixtures of DMAB and HABT with relative weights determined by the dwell time for HABT and DMAB states.

Line-Shape Evidence. We also observe that the stepped transitions of DMAB are accompanied by the changes in lineshapes. Figure 7a and b display a mild trajectory (k_{NBT} = 0.046 s^{-1}) of a DMAB peak (ν_3) and its intensity profile, in which we observe that the intensity steps (for example, δ = 0.095 in Figure 7a) accompany spectral change between a singlet and doublet peaks (see the points 3, 4, and 5 of Figure 7b and c). These strongly support that the step-transition corresponds to the chemical transformation of one of the two DMAB molecules under two different heterogeneous surface states.[61] Additionally, the singlet peak has a significantly narrower line width (Figure 7c) than that of typical, heterogeneously broadened ν_{NO} peak of NBT (∼9 cm^{-1} vs ∼21 cm^{-1}), indicating that the spectra arise from very few number of DMAB molecules.

2.4. Modeling of SMSERS Trajectories. By combining the electrodynamics calculation of local field enhancement, and the Monte Carlo simulation of 2-dimensional surface photochemistry, we have modeled the SERS trajectories. By comparing the model and the experimental trajectories, we attempt to answer the following three questions: (1) Does the plasmonically enhanced Raman signal of a single molecule *quantitatively* explain the magnitude of SERS steps observed? (2) What is the origin of the finite distribution of the step sizes? (3) Could the reaction events of individual molecules qualitatively explain the observed time-evolution of SERS signals?

2.4.1. Position-Dependent Raman Enhancement. The electromagnetically (EM) enhanced Raman signal of a DMAB at (x, y) near the junction center (0, 0) can be modeled by

$$\begin{aligned}\Delta_{DMAB}(x, y) &= \sigma_{DMAB}|E_{loc}(\omega_0, x, y)/E_0|^2 \\ &\quad \times |E_{loc}(\omega_{DMAB}, x, y)/E_0|^2 \\ &= \sigma_{DMAB}F_{DMAB}(x, y) \end{aligned} \quad (1)$$

DOI: 10.1021/jacs.6b01865
J. Am. Chem. Soc. 2016, 138, 4673−4684

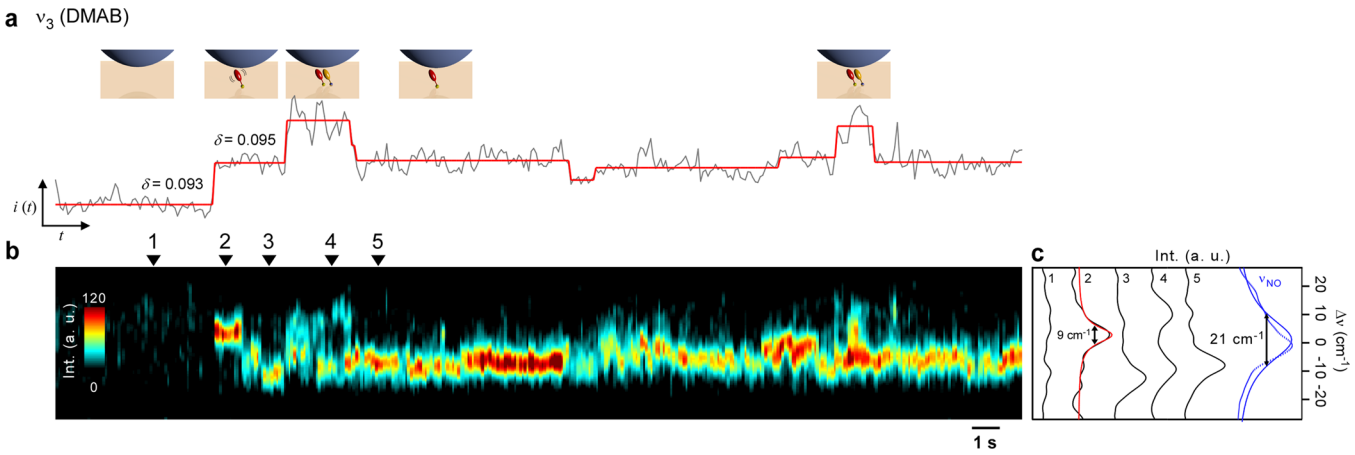

Figure 7. Spectral evidence of single-molecule reaction events. (a) Normalized SERS trajectory ($i_{DMAB}(t)$, gray) of DMAB and the fit (red) to step functions. (b) The corresponding SERS spectra. (c) Sampling of the instantaneous spectra of ν_3 (DMAB) (indicated by numerals in (b)) shown in (b) together with a fits to Lorentzian functions. The inset cartoons in (a) schematically show the evolution of the number of DMAB molecules (red and orange spheroids) during the reaction. Molecules in different states are depicted in different colors.

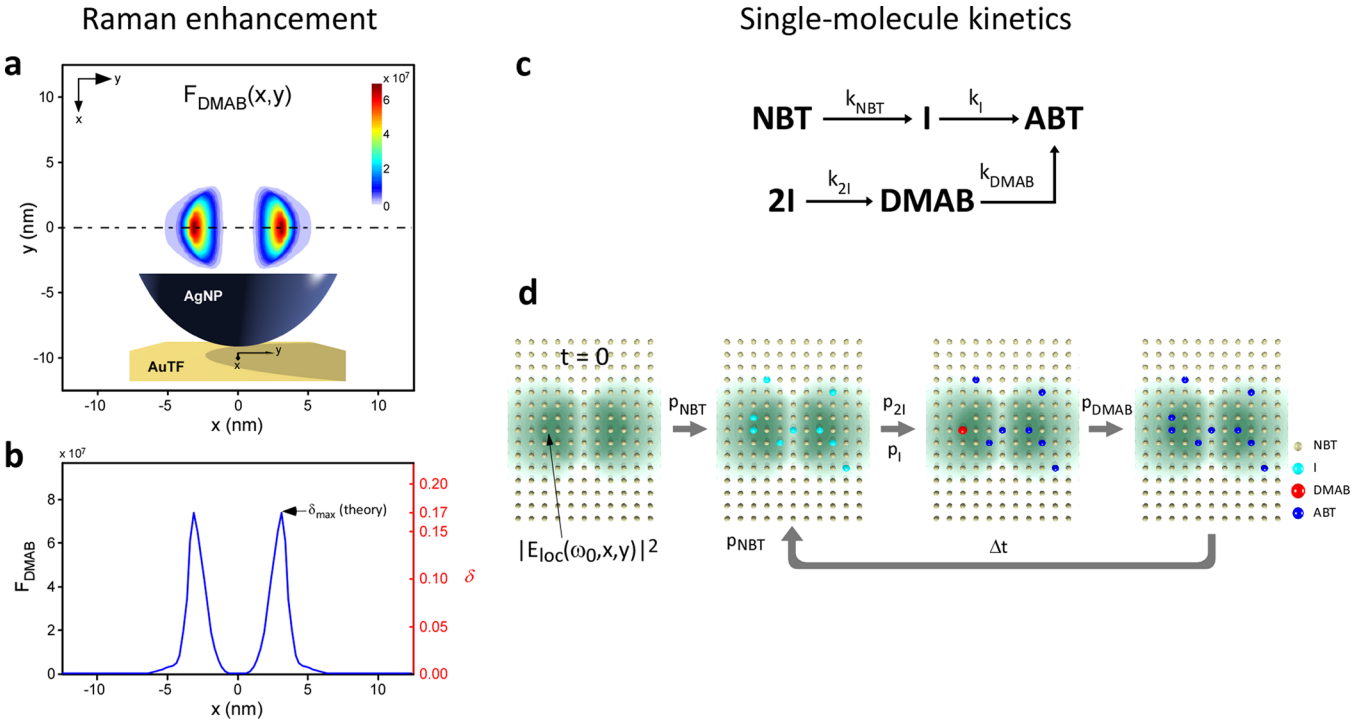

Figure 8. Modeling of single-molecule SERS intensities and single-molecule surface kinetics. (a) Position-dependent SERS enhancement factor for ν_3 peak of DMAB, $F_{DMAB}(x, y)$, simulated by FDTD method. (b) The line profile of $F_{DMAB}(x, y)$ (left y-axis) along the center of the junction (shown in dash-dot line in (a)), and the theoretical SERS intensity of DMAB (δ, right y-axis). Also indicated by an arrow is the position in the sample exhibiting the maximum single-molecule SERS signal. (c) Simplified reaction kinetics model of the plasmon-assisted reduction of NBT. (d) Schematic of Monte Carlo simulation of single-molecule kinetics. At time zero (t = 0), NBT molecules (yellow spheres) occupy all of the adsorption sites. For each time step (Δt), reaction steps occur stochastically with probabilities p_{NBT}, p_I, p_{2I}, and p_{DMAB}. The p_{NBT} and p_{DMAB} are dependent on the local field intensity, $|E_{loc}(\omega_0, x, y)|^2$ (shown in green colors), which sensitively changes for different molecular adsorption sites (x, y). For each cycle, the SERS intensities of NBT and DMAB are evaluated based on the occupation states of each adsorption site and the Raman enhancement factors.

where $E_{loc}(\omega_0, x, y)$, $E_{loc}(\omega_{DMAB}, x, y)$, and E_0 are the local field at the laser excitation frequency (ω_0), the local field at the Stokes–Raman frequency of DMAB (ω_{DMAB}), and the incident laser field, respectively. The $F_{DMAB}(x, y) = |E_{loc}(\omega_0, x, y)/E_0|^2|E_{loc}(\omega_{DMAB}, x, y)/E_0|^2$ is the single-molecule Raman enhancement factor (see Figure 8a for the finite-difference time-domain (FDTD) simulation of $F_{DMAB}(x, y)$), and σ_{DMAB} is the Raman cross-section of a DMAB molecule at ν_3 = 1445 cm^{-1}. Analogously, the reference signal, $I_{0,NBT}$, is modeled as the sum of SERS signals of all NBT molecules near the junction position: $I_{0,NBT} = \sigma_{NBT}N_{NBT}\langle F_{NBT}\rangle$, where N_{NBT} is the number of NBT molecules experiencing an enhanced field, and $\langle F_{NBT}\rangle$ is the enhancement factor for NBT averaged over the junction area. The σ_{NBT} is the Raman

DOI: 10.1021/jacs.6b01865
J. Am. Chem. Soc. 2016, 138, 4673−4684

cross-section of NBT at ν_{NO} = 1347 cm^{-1}. The normalized SERS signal of a single DMAB is thus calculated as follows:

$$\delta(x, y) = \frac{\Delta_{DMAB}(x, y)}{I_{0,NBT}} = \frac{\sigma_{DMAB}}{\sigma_{NBT}} \times \frac{1}{N_{NBT}\langle F_{NBT}\rangle} \times F_{DMAB}(x, y) \quad (2)$$

Figure 8b shows a line profile of $F_{DMAB}(x, y)$ and δ (x, y) sampled along a line crossing the center of the AgNP-AuTF junction, illustrating the drastic variation of SERS enhancement with respect to the location of the molecule around the center of hotspot. In particular, it reveals that a DMAB placed at surface sites with $F_{DMAB} > 1.4 \times 10^7$ can yield a normalized SMSERS signal with a range of δ = 0.03−0.17. The maximum SMSERS signal, δ_{max} = 0.17 (corresponding to $F_{DMAB} = 1.1 \times 10^8$), occurs for a DMAB placed at the hottest site in a given junction. This range of δ agrees with the experimental range of steps δ = 0.03−0.8 (Figure 3c, hot and mild distributions).

2.4.2. Monte Carlo Simulation of Reactive SERS Trajectories. To confirm that the dynamics of the steps represents the genuine reaction kinetics, and to understand the shapes of the δ-distributions, we carried out a Monte Carlo simulation of reactive SERS trajectories of DMAB. On the basis of the ensemble rate law analysis of hot trajectories above (see section 2.2.2), we setup a simplified kinetics model (Figure 8c, Supporting Information E) in which there is only one type of short-lived intermediate (I) generated from NBT, and the NBT → I (k_{NBT}) and DMAB → 2ABT (k_{DMAB}, corresponding to the k_2 in the above rate law analysis) steps are the rate-determining steps (k_{NBT}, $k_{DMAB} \ll k_1$, k_{2I}). Using the simplified kinetic pathways, we conduct a Monte Carlo simulation[62,63] of the single-molecule reaction (see Figure 8d and Materials and Methods), in which individual NBTs immobilized on a AuTF undergo stochastic transformations with probability, p_A, for each reaction step-A. Particularly, p_{NBT} and p_{DMAB} are modeled as $p_{X=NBT\ or\ DMAB}(x, y) = 1 - \exp(-a_X f|E_{loc}(\omega_0, x, y)|^2\Delta t)$, where a_X is a constant, and the Δt = 1 ms is the time-step. This form takes into account the E_{loc}-dependent plasmonic hot-electron transfer rates, which are dependent on the local field intensity. The f is a variable that approximately models the junction-to-junction variation in $\langle|E_{loc}(\omega_0)|^2\rangle$. For each Δt, the normalized SERS signal $i(t)$ from a junction is calculated from the occupation states of each adsorption sites, Raman enhancement factors, and the experimental Raman scattering cross sections.

The three sets of simulated SERS trajectories in Figure 2g−i, which differ only in terms of the $\langle|E_{loc}(\omega_0)|^2\rangle$ (f = 1, 0.04, and 0.008 for (g), (h) and (i), respectively), reproduce key features of the hot, mild, and cold trajectories shown in Figure 2d−f. Particularly, the simulated hot trajectory shown in Figure 2g, involving ∼20 DMABs (see inset for DMAB distribution (dots in red) and the local field distribution(distribution in green)), is composed of many cumulative steps, resulting in a shape approximating the ensemble rate-law equation. On the other hand, the mild trajectory (Figure 2h), which involves <4 DMABs, shows a few on/off transitions. Figure 3d shows corresponding δ-distributions of the simulated hot and mild trajectories of DMAB (Figure 2g and h), reproducing both the qualitative and quantitative features of the experimental δ-distributions in Figure 3c: The model distribution for mild trajectories shows a peak at δ_{mp} = 0.13 (experiment, δ_{mp} = 0.2) whereas the one for the hot trajectories shows a monotonically decaying shape. Such features appear in a δ-range that agrees with the experimental result within a factor of 3, which is remarkable given that the model takes into account only the field-enhancement of an idealized nanosphere−thin film junction and the experimental Raman cross sections of NBT and DMAB. Whereas the model δ-distributions are tightly bound by δ_{max}, the upper-bounds of experimental distributions are rather diffuse. This blurring may be caused by the finite dispersion of nanoparticle size and shape, causing variation in the spatial shapes of the E_{loc}.

The shape differences in the δ-distributions of hot and mild trajectories reflect the difference in the spatial distributions of DMABs generated under different reaction conditions (see inset of Figure 3d for cumulative spatial distribution of photogenerated DMAB). The formation of DMAB needs two neighboring plasmon-generated intermediates (I), each with a formation probability proportional to $|E_{loc}(\omega_0, x, y)|^2$. Therefore, when the reactant depletion is negligible (mild trajectories), the spatial distribution of DMABs is tightly focused near the hottest site. On the other hand, when there is a significant depletion of reactants during the reaction (hot trajectories), the spatial distribution of DMAB is loosely focused. This explains why the two Monte Carlo-simulated δ-distributions appear similar to those calculated for DMABs following a $|E_{loc}(\omega_0, x, y)|^4$ spatial distribution (approximating mild trajectories) and for uniformly distributed DMABs (hot trajectories) (see the dashed lines in Figure 3d). Overall, the simulation reproduces the time-evolution of SERS trajectories, the magnitude of step intensities, and their distributions in terms of single-molecular reaction events around a plasmonic junction, further supporting our interpretation.

2.5. Conclusions. The result clearly demonstrates that SERS can follow the single-molecule surface reaction events in real time: The reactants immobilized at the junctions of nanoparticle−thin film structures produce time-resolved SERS spectra with discrete step-transitions of photoproducts. The yield, dynamics, and the magnitudes of such steps can be fully explained and modeled by the surface chemistry and plasmon-enhanced Raman signals of individual molecules. The frequency-domain features associated with the step-transitions further reveal the heterogeneous environment and the existence of short-lived intermediates. We find that plasmonic junctions with an enhancement of ∼10^8, which is easily achievable in many other forms of plasmonic junctions, are already sufficient to record time-resolved (∼10 ms resolution) SERS spectra of individual reacting molecules with a Raman cross-section of $\sigma \sim 10^{-28}$ cm^2/sr.

The result also constitutes the most direct assessment of SMSERS *intensity* thus far. The plasmon-assisted reaction creates immobilized single molecules preferentially at the hottest sites of a junction, and the SMSERS signals thus generated are predictable and their intensities do not randomly fluctuate in time. Their intensities can be quantitatively (within 1 order of magnitude) explained by the plasmonic enhancement around the junction. This confirms that much of the randomness found in generic SMSERS signals can be removed if we could confine the positions of target molecules near the centers of well-defined hotspots.

The applicability of the method to a more general class of catalytic reactions is largely limited by the Raman cross sections of the chemical species involved, the plasmonics of metallic junctions, and the accessibility of the molecules to the hottest part of the junctions in a controllable fashion. By implementing

DOI: 10.1021/jacs.6b01865
J. Am. Chem. Soc. 2016, 138, 4673−4684

chemical and physical methods to spatially confine the molecules to the centers of hotspots (for example, by host–guest chemistry[21]), and by employing nanoparticles with better-defined geometries (such as nanocubes or octahedrons[64] or shell-isolated nanoparticles[65]), we will be able to further widen the range of surface reactions that can be studied through SMSERS.

3. MATERIALS AND METHODS

3.1. Sample. A fully saturated self-assembled monolayer of 4-nitrobenzenethiols (NBT, Tokyo Chemical Industry Co., Ltd.; used without further purification) is formed on top of a Au thin-film (TF; Au thin film with a thickness of 10 nm formed on top of a Ti adhesion layer of 2 nm) formed on a glass substrate. The Ag nanoparticles (AgNPs, diameters of 80 nm, BBI Co., Ltd.) are dispersed on top of the NBT/AuTF surface to form NP-NBT-AuTF junctions.

3.2. Measurement. The SERS signals were measured with a home-built epi-confocal Raman/atomic force microscope (AFM) equipped with a high-NA objective lens (Plan Apochromat, 60×, 1.45 NA, Olympus), a Raman spectrometer (500im, focal length = 50 cm, Chromex; EM-CCD, iXon3 897, Andor Tech), a piezo-scanner (P-500.3, Physik Instrumente) and a HeNe laser (λ_{ex} = 633 nm, Melles Griot, < 1 mW) as the excitation light source. SERS trajectories are obtained by placing the laser focus onto a single AuNP-ABT-AuTF junction and recording the SERS spectra as a function of time (30 ms exposure time/spectrum).

3.3. Monte Carlo Simulation. In the model, the NBTs are immobilized at two-dimensional grid points (ai, aj) on a Au-surface (Figure 4d), where a = 0.6144 nm is the intermolecular distance of NBTs close-packed on the surface, and (i, j) are integers. The reaction probability of single molecules for each reaction step A, is defined as $p_A(x, y) = 1 - exp(-k_A\Delta t)$. The probabilities for the two rate-determining steps are described in the main text. The 2I → DMAB step occurs with a unit probability ($p_{2I} = 1$) only when there are two or more neighboring I's. The values of other parameters, a_{NBT} = 1.0 ms^{-1}, a_{DMAB} = 0.26 ms^{-1}, p_I = 0.005 and Δt (time-step) = 1 ms, are chosen such that the strong field limit of the simulation mimic the hot trajectories, and their reaction branching between direct and indirect paths. For each Δt, we calculate the stochastic reaction events, and evaluate the SERS signal of the NBT and DMAB molecules as $S_{X=DMAB\ or\ NBT}(t) = \sum_{i,j} n_{i,j,X}(t)F_X(ai, aj)$, where $n_{i,j,X}(t) = 0, 1$ is the occupation state of X at site (i, j) at time t. The $F_X(ai, aj)$ is the SERS enhancement factor at (ai, aj) for X as defined in the main text. The normalized time-dependent SERS trajectory of NBT and DMAB is thus calculated as $i_X(t) = (\sigma_X/\sigma_{NBT}) \cdot S_X(t)/S_{NBT}(0)$.

ASSOCIATED CONTENT

Supporting Information

The Supporting Information is available free of charge on the ACS Publications website at DOI: 10.1021/jacs.6b01865.

(A) Raman scattering enhancement factors, (B) Relative surface coverage of ABT, NBT, and DMAB, and the reaction branching during the photoreaction, (C) Peak assignment of NBT and DMAB molecule, (D) Estimation of relative Raman cross sections of NBT, DMAB, and ABT molecules, (E) Kinetic rate law analysis of NBT photoreduction, (F) Correlations between the step-transition frequencies of DMAB and the decay rate of NBT, (G) Influence of blocking and unblocking the laser beam during the photocatalytic reaction, (H) Cross-correlation analysis of SERS trajectory, (I) Density-functional theory calculation of Raman spectra of possible reaction intermediates, (J) Analytical data on the 4,4′-dimercaptoazobenzene (DMAB). (PDF)

AUTHOR INFORMATION

Corresponding Author

*zhkim@snu.ac.kr

Notes

The authors declare no competing financial interest.

ACKNOWLEDGMENTS

The work is supported by the SNU grant (Research Resettlement Fund for the new faculty of SNU), and by the BioNano Health-Guard Research Center funded by the Ministry of Science, and ICT & Future Planning (MSIP) of Korea as Global Frontier Project (H-GUARD_2013M3A6B2078947). We thank J. W. J. Kerssemakers for sharing the step-fitting codes.

REFERENCES

(1) Roeffaers, M. B. J.; Sels, B. F.; Uji-i, H.; De Schryver, F. C.; Jacobs, P. A.; De Vos, D. E.; Hofkens, J. *Nature* **2006**, *439*, 572.
(2) Roeffaers, M. B. J.; De Cremer, G.; Uji-i, H.; Muls, B.; Sels, B. F.; Jacobs, P. A.; De Schryver, F. C.; De Vos, D. E.; Hofkens, J. *Proc. Natl. Acad. Sci. U. S. A.* **2007**, *104*, 12603.
(3) Andoy, N. M.; Zhou, X.; Choudhary, E.; Shen, H.; Liu, G.; Chen, P. *J. Am. Chem. Soc.* **2013**, *135*, 1845.
(4) Cordes, T.; Blum, S. A. *Nat. Chem.* **2013**, *5*, 993.
(5) Sambur, J. B.; Chen, P. *Annu. Rev. Phys. Chem.* **2014**, *65*, 395.
(6) Decan, M. R.; Impellizzeri, S.; Marin, M. L.; Scaiano, J. C. *Nat. Commun.* **2014**, *5*, 4612.
(7) Schlücker, S. *Angew. Chem., Int. Ed.* **2014**, *53*, 4756.
(8) Stiles, P. L.; Dieringer, J. A.; Shah, N. C.; Duyne, R. P. V. *Annu. Rev. Anal. Chem.* **2008**, *1*, 601.
(9) Harvey, C. E.; Weckhuysen, B. M. *Catal. Lett.* **2015**, *145*, 40.
(10) Moskovits, M. *Phys. Chem. Chem. Phys.* **2013**, *15*, 5301.
(11) Kneipp, K.; Wang, Y.; Kneipp, H.; Perelman, L. T.; Itzkan, I.; Dasari, R. R.; Feld, M. S. *Phys. Rev. Lett.* **1997**, *78*, 1667.
(12) Xu, H.; Bjerneld, E. J.; Käll, M.; Börjesson, L. *Phys. Rev. Lett.* **1999**, *83*, 4357.
(13) Le Ru, E. C.; Meyer, M.; Etchegoin, P. G. *J. Phys. Chem. B* **2006**, *110*, 1944.
(14) Dieringer, J. A.; Lettan, R. B.; Scheidt, K. A.; Van Duyne, R. P. *J. Am. Chem. Soc.* **2007**, *129*, 16249.
(15) Ward, D. R.; Halas, N. J.; Ciszek, J. W.; Tour, J. M.; Wu, Y.; Nordlander, P.; Natelson, D. *Nano Lett.* **2008**, *8*, 919.
(16) Haran, G. *Acc. Chem. Res.* **2010**, *43*, 1135.
(17) Le Ru, E. C.; Etchegoin, P. G. *Annu. Rev. Phys. Chem.* **2012**, *63*, 65.
(18) Mirsaleh-Kohan, N.; Iberi, V.; Simmons, P. D.; Bigelow, N. W.; Vaschillo, A.; Rowland, M. M.; Best, M. D.; Pennycook, S. J.; Masiello, D. J.; Guiton, B. S.; Camden, J. P. *J. Phys. Chem. Lett.* **2012**, *3*, 2303.
(19) Kitahama, Y.; Araki, D.; Yamamoto, Y. S.; Ito, T.; Ozaki, Y. *Phys. Chem. Chem. Phys.* **2015**, *17*, 21204.
(20) Zhang, Z.; Deckert-Gaudig, T.; Singha, P.; Deckert, V. *Chem. Commun.* **2015**, *51*, 3069.
(21) Taylor, R. W.; Coulston, R. J.; Biedermann, F.; Mahajan, S.; Baumberg, J. J.; Scherman, O. A. *Nano Lett.* **2013**, *13*, 5985.
(22) Nie, S.; Emory, S. R. *Science* **1997**, *275*, 1102.
(23) Cortés, E.; Etchegoin, P. G.; Le Ru, E. C.; Fainstein, A.; Vela, M. E.; Salvarezza, R. C. *J. Am. Chem. Soc.* **2010**, *132*, 18034.
(24) El-Khoury, P. Z.; Hu, D.; Apkarian, V. A.; Hess, W. P. *Nano Lett.* **2013**, *13*, 1858.
(25) Shegai, T.; Vaskevich, A.; Rubinstein, I.; Haran, G. *J. Am. Chem. Soc.* **2009**, *131*, 14390.
(26) Sonntag, M. D.; Chulhai, D.; Seideman, T.; Jensen, L.; Van Duyne, R. P. *J. Am. Chem. Soc.* **2013**, *135*, 17187.
(27) Park, W.-H.; Kim, Z. H. *Nano Lett.* **2010**, *10*, 4040.
(28) Stranahan, S. M.; Willets, K. A. *Nano Lett.* **2010**, *10*, 3777.
(29) van Schrojenstein Lantman, E. M.; de Peinder, P.; Mank, A. J. G.; Weckhuysen, B. M. *ChemPhysChem* **2015**, *16*, 547.

DOI: 10.1021/jacs.6b01865
J. Am. Chem. Soc. 2016, 138, 4673–4684

(30) Joseph, V.; Engelbrekt, C.; Zhang, J.; Gernert, U.; Ulstrup, J.; Kneipp, J. *Angew. Chem., Int. Ed.* **2012**, *51*, 7592.
(31) Kim, K.; Choi, J.-Y.; Shin, K. S. *J. Phys. Chem. C* **2014**, *118*, 11397.
(32) Sun, M.; Zhang, Z.; Zheng, H.; Xu, H. *Sci. Rep.* **2012**, *2*, 647.
(33) Zhao, L.-B.; Chen, J.-L.; Zhang, M.; Wu, D.-Y.; Tian, Z.-Q. *J. Phys. Chem. C* **2015**, *119*, 4949.
(34) Zhao, L.-B.; Zhang, M.; Huang, Y.-F.; Williams, C. T.; Wu, D.-Y.; Ren, B.; Tian, Z.-Q. *J. Phys. Chem. Lett.* **2014**, *5*, 1259.
(35) Zhao, L.-B.; Zhang, M.; Ren, B.; Tian, Z.-Q.; Wu, D.-Y. *J. Phys. Chem. C* **2014**, *118*, 27113.
(36) van Schrojenstein Lantman, E. M.; Deckert-Gaudig, T.; Mank, A. J. G.; Deckert, V.; Weckhuysen, B. M. *Nat. Nanotechnol.* **2012**, *7*, 583.
(37) Nordlander, P.; Le, F. *Appl. Phys. B: Lasers Opt.* **2006**, *84*, 35.
(38) Mertens, J.; Eiden, A. L.; Sigle, D. O.; Huang, F.; Lombardo, A.; Sun, Z.; Sundaram, R. S.; Colli, A.; Tserkezis, C.; Aizpurua, J.; Milana, S.; Ferrari, A. C.; Baumberg, J. J. *Nano Lett.* **2013**, *13*, 5033.
(39) Hu, J.; Tanabe, M.; Sato, J.; Uosaki, K.; Ikeda, K. *J. Am. Chem. Soc.* **2014**, *136*, 10299.
(40) Ikeda, K.; Suzuki, S.; Uosaki, K. *J. Am. Chem. Soc.* **2013**, *135*, 17387.
(41) Benz, F.; Tserkezis, C.; Herrmann, L. O.; de Nijs, B.; Sanders, A.; Sigle, D. O.; Pukenas, L.; Evans, S. D.; Aizpurua, J.; Baumberg, J. J. *Nano Lett.* **2015**, *15*, 669.
(42) Mubeen, S.; Zhang, S.; Kim, N.; Lee, S.; Krämer, S.; Xu, H.; Moskovits, M. *Nano Lett.* **2012**, *12*, 2088.
(43) Di Martino, G.; Tappertzhofen, S.; Hofmann, S.; Baumberg, J. *Small* **2016**, *12*, 1334.
(44) Kim, K.; Lee, I. *Langmuir* **2004**, *20*, 7351.
(45) Shin, K. S.; Park, C. S.; Kang, W.; Kim, K. *Chem. Lett.* **2008**, *37*, 180.
(46) Dong, B.; Fang, Y.; Xia, L.; Xu, H.; Sun, M. *J. Raman Spectrosc.* **2011**, *42*, 1205.
(47) Xie, W.; Walkenfort, B.; Schlücker, S. *J. Am. Chem. Soc.* **2013**, *135*, 1657.
(48) Dong, B.; Fang, Y.; Chen, X.; Xu, H.; Sun, M. *Langmuir* **2011**, *27*, 10677.
(49) Xie, W.; Herrmann, C.; Kömpe, K.; Haase, M.; Schlücker, S. *J. Am. Chem. Soc.* **2011**, *133*, 19302.
(50) Zhang, Z.; Fang, Y.; Wang, W.; Chen, L.; Sun, M. *Advanced Science* **2016**, *3*, 1500215.
(51) Knight, M. W.; Sobhani, H.; Nordlander, P.; Halas, N. J. *Science* **2011**, *332*, 702.
(52) Zheng, B. Y.; Zhao, H.; Manjavacas, A.; McClain, M.; Nordlander, P.; Halas, N. J. *Nat. Commun.* **2015**, *6*, 7797.
(53) Mukherjee, S.; Libisch, F.; Large, N.; Neumann, O.; Brown, L. V.; Cheng, J.; Lassiter, J. B.; Carter, E. A.; Nordlander, P.; Halas, N. J. *Nano Lett.* **2013**, *13*, 240.
(54) van Schrojenstein Lantman, E. M.; Gijzeman, O. L. J.; Mank, A. J. G.; Weckhuysen, B. M. *ChemCatChem* **2014**, *6*, 3342.
(55) Kerssemakers, J. W. J.; Laura Munteanu, E.; Laan, L.; Noetzel, T. L.; Janson, M. E.; Dogterom, M. *Nature* **2006**, *442*, 709.
(56) Weiss, A.; Haran, G. *J. Phys. Chem. B* **2001**, *105*, 12348.
(57) Imabayashi, S.-i.; Hobara, D.; Kakiuchi, T. *Langmuir* **2001**, *17*, 2560.
(58) Noda, I.; Ozaki, Y. In *Two-Dimensional Correlation Spectroscopy—Applications in Vibrational and Optical Spectroscopy*; John Wiley & Sons, Ltd: New York, 2005.
(59) Tallarida, N.; Rios, L.; Apkarian, V. A.; Lee, J. *Nano Lett.* **2015**, *15*, 6386.
(60) Park, K.-D.; Muller, E. A.; Kravtsov, V.; Sass, P. M.; Dreyer, J.; Atkin, J. M.; Raschke, M. B. *Nano Lett.* **2016**, *16*, 479.
(61) Etchegoin, P. G.; Le Ru, E. C. *Anal. Chem.* **2010**, *82*, 2888.
(62) Santos, D. P. d.; Andrade, G. F. S.; Temperini, M. L. A.; Brolo, A. G. *J. Phys. Chem. C* **2009**, *113*, 17737.
(63) Le Ru, E. C.; E, P. G.; Meyer, M. *J. Chem. Phys.* **2006**, *125*, 204701.
(64) Heo, J.; Kim, D.-S.; Kim, Z. H.; Lee, Y. W.; Kim, D.; Kim, M.; Kwon, K.; Park, H. J.; Yun, W. S.; Han, S. W. *Chem. Commun.* **2008**, 6120.
(65) Li, J. F.; Huang, Y. F.; Ding, Y.; Yang, Z. L.; Li, S. B.; Zhou, X. S.; Fan, F. R.; Zhang, W.; Zhou, Z. Y.; WuDe, Y.; Ren, B.; Wang, Z. L.; Tian, Z. Q. *Nature* **2010**, *464*, 392.

DOI: 10.1021/jacs.6b01865
J. Am. Chem. Soc. 2016, 138, 4673−4684